Epitaxially-Stacked High Efficiency Laser Diodes Near 905 nm

Yuliang Zhao, Guowen Yang, Yongming Zhao, Song Tang, Yu Lan, Yuxian Liu, Zhenfu Wang, and Abdullah Demir

***Abstract*—We report on studying tunnel junctions and an optical cavity structure for developing epitaxially-stacked high-efficiency 905 nm high-power laser diodes. The GaAs tunnel junctions were explored via simulations and experiments to realize a high peak current density of 7.7 × 10^4 A/cm^2 and a low specific resistance of 1.5 × 10^{-5} Ωcm^2 with a high n-doping concentration of 6 × 10^{19} cm^{-3}. Employing a low-loss epitaxial structure design, single-, double-, and triple-cavity structure laser diodes demonstrated power scaling by epitaxial stacking. Triple-cavity laser diodes have a low optical loss (0.42 cm^{-1}) and generate a peak power of 83 W with a short cavity length of 750 μm at a limited current of 30 A.**

***Index Terms*—Epitaxial stacking, high efficiency, laser diode, low optical loss, n-doping concentration, power scaling, specific resistance, tunnel junction.**

I. Introduction

HIGH-power continuous-wave (CW) and quasi-continuous-wave (QCW) laser diodes (LDs) have been widely employed as pump sources for fiber and solid-state lasers [1], [2], [3]. Recently, high-power pulsed laser diodes evolved beyond these fields with demands in three-dimensional (3D) sensing and light detection and ranging (LiDAR) applications [4], [5], [6]. Depending on the method employed and application, the systems involve ∼1–100 ns long pulses with peak power levels of 10 to 100 W [6]. However, it is challenging to generate short electrical pulses with high current amplitude [7]. To circumvent this issue, several separate and relatively independent LDs can be monolithically stacked in series by tunnel junctions (TJs). Ideally, the internal quantum efficiency of such epitaxially stacked LDs is linearly proportional to the number of diodes, N, so that the laser output power will be scaled by N at a given current. In this approach, the drawback would be scaling the applied voltage by the same factor, assuming no voltage penalty with the TJs. Also, LiDAR systems have spectral requirements with preferred laser emission near 905 or 1550 nm. Automotive LiDARs commonly employ 905 nm due to the low-cost off-the-shelf components, including high-power GaAs-based LDs with pulsed operation near 905 nm and silicon photodetectors [8].

Since Esaki's discovery of the tunneling effect in 1958 [9], TJs have been intensively investigated and widely employed in solar cells. However, their investigation in epitaxially stacked LDs have been limited [10], [11], [12], [13], [14], [15]. Rather than stacking individual LDs [16], epitaxial stacking is desirable since it can simplify packaging and is cost-effective. Relatively long cavity length lasers (≥2.5 mm) have been demonstrated in the form of microarray with short pulse operation power levels above 100 W [12] and for 1-cm wide bars with QCW output power levels above 1 kW [13], [14], [15]. OSRAM reported 905 nm pulsed LDs with a peak output power of 125 W using vertically integrated three emitters with PCE of 28.4% at 40 A [17]. Additionally, epitaxial stacking of several active regions in a single waveguide core with a third-order optical mode was demonstrated to utilize surface grating for wavelength locking, with ∼3 W output power achieved [18], [19]. Such epitaxial stacking with TJ has been applied for VCSELs as well [20], [21]. For the TJs, it is beneficial to have a simple material structure (e.g., GaAs) for epitaxial growth and high doping concentration to obtain low specific resistance [22]. Optical cavities with very low internal optical loss should be employed for high slope efficiency. Low internal optical losses of 0.31 cm^{-1} for single-cavity LD [23] and 0.7 cm^{-1} for triple-cavity LD [18] were demonstrated. For the extensive use of edge-emitting LDs in LiDAR applications, utilizing a short laser cavity is desirable for a low cost. In this work, we aimed to realize low resistance GaAs TJs and low internal loss optical cavities and then effectively combine them to achieve high-efficiency epitaxially-stacked LDs with short cavity lengths, which is lacking in the literature.

The paper, first, focuses on the experiment and simulation of TJs with various high n-doping concentrations. The simulations are calibrated by the experimentally measured J-V curves that

Manuscript received 20 September 2022; accepted 29 September 2022. Date of publication 4 October 2022; date of current version 19 October 2022. This work was supported in part by the National Natural Science Foundation of China under Grant 61504167, in part by the Natural Science Foundation of Shaanxi Province, China under Grants 2019ZY-CXPT-03-05, 2018JM6010 and 2015JQ6263 and in part by the Talent Project of Science and Technology Department of Shaanxi Province under Grant 2017KJXX-72. *(Corresponding authors: Guowen Yang; Abdullah Demir.)*

Yuliang Zhao, Guowen Yang, Yu Lan, and Yuxian Liu are with the State Key Laboratory of Transient Optics and Photonics, Xi'an Institute of Optics and Precision Mechanics, Chinese Academy of Sciences, Xi'an 710119, China, and also with the University of Chinese Academy of Sciences, Beijing 100049, China (e-mail: zhaoyuliang2016@opt.cn; yangguowen@opt.cn; lanyu2017@opt.cn; liuyuxian2017@opt.cn).

Yongming Zhao and Song Tang are with the Dogain Laser Technology (Suzhou) Company, Ltd, Suzhou 215123, China (e-mail: zhaoym@dogain.com; tangs@dogain.com).

Zhenfu Wang is with the State Key Laboratory of Transient Optics and Photonics, Xi'an Institute of Optics and Precision Mechanics, Chinese Academy of Sciences, Xi'an 710119, China (e-mail: wzf2718@opt.ac.cn).

Abdullah Demir is with the UNAM - Institute of Materials Science and Nanotechnology, Bilkent University, 06800 Ankara, Turkey (e-mail: demirab@gmail.com).

Digital Object Identifier 10.1109/JPHOT.2022.3211964

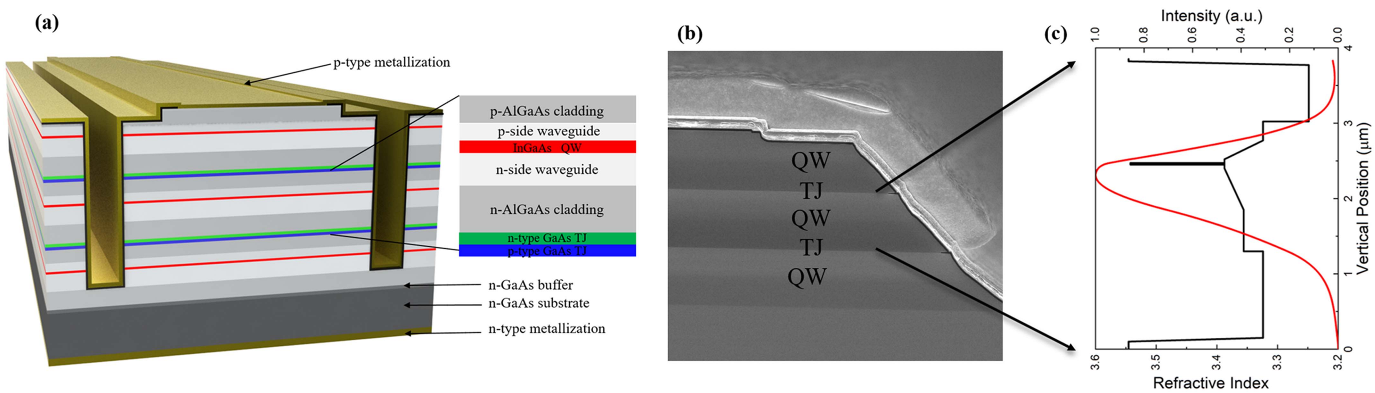

Fig. 1. (a) The schematic and (b) SEM picture of 3-cavity LD. (c) Profiles of refractive index and calculated optical intensity of the vertical mode of single p-i-n structure.

demonstrated very high peak current density and low specific resistance. Then, we employed the TJs for epitaxial stacking of LDs and obtained a record low optical loss of 0.42 cm^{-1} for a triple-cavity LD showing TJ incorporation without introducing loss. Triple-cavity LDs (750 μm long and 200 μm wide waveguide) achieve high peak power of 83 W at a limited current of 30 A (100 ns, 100 Hz).

II. Structure Design

The LDs with one, two, and three p-i-n junctions have been investigated in this work. Fig. 1(a) shows the schematic of a 3-cavity diode laser, where two reverse biased TJs connect three optically independent laser cavities. LD wafers with 1-, 2-, and 3-cavity were epitaxially grown by metal-organic chemical vapor deposition (MOCVD) and fabricated by a standard LD fabrication process. TJ can provide electrical coupling with negligible optical loss by properly designing the epitaxial structure. Fig. 1(b) shows the scanning electron microscopy (SEM) picture of the fabricated 3-cavity LD. The refractive index and optical mode profile of a 1-cavity is shown in Fig. 1(c). A GRINSCH (graded-index separate confinement heterostructure) vertical cavity design is used to obtain high carrier injection efficiency, and a thin p-waveguide is employed for low optical absorption loss. The active region has two InGaAs quantum wells to increase the optical confinement factor and improve the modal gain for short cavity lengths.

The material quality and electrical characteristics of TJs are critical for the overall efficiency of the epitaxially stacked LD. Using a combination of numerical simulation and experimental results, first, we examined the critical parameters of TJs, such as peak tunneling current density and electrical resistance, as a function of doping concentration. Usually, TJ consists of a heavily doped p-n junction with a typical doping concentration higher than 10^{19} cm^{-3}. For effective device operation, TJ must form a low resistance path for carriers between the p and n terminal of its neighbor optical cavities. A low resistance ensures a minimal voltage drop and hence a minimal influence on the optoelectronic performance of the device.

The TJ test structures were epitaxially grown on an n-GaAs substrate with a 500 nm n-GaAs buffer layer (3×10^{18} cm^{-3}), a 25 nm Te-doped n++ GaAs with various doping concentrations of 4×10^{19}, 5×10^{19}, and 6×10^{19} cm^{-3}, a 25 nm C-doped p++ GaAs (1×10^{20} cm^{-3}) and finalized with p++ GaAs contact layer (p>5×10^{19} cm^{-3}). Since the p-doping reaches a high level of 1×10^{20} cm^{-3} with a C dopant, we focus on investigating the n-doping concentration optimization using the Te dopant. The material and thickness were chosen considering the material quality and device performance [24]. Te and C were used due to their low diffusion coefficient and high doping concentration. Hence, thin TJ layers are possible, which is advantageous for the minimal impact of these layers on the optical mode profile and optical loss. The TJ structures were fabricated employing a standard process with metal contacts for electrical testing and cleaved into chips with a size of (200 μm) $\times$ (400 μm). Fig. 2(a) shows the simulated and experimental current density versus voltage (J-V) curves. The JV curves with solid lines in Fig. 2(a) present the experimental electrical characteristics of the TJs tested in V-I mode by a current source. In Fig. 2(a), the positive voltage demonstrates the forward bias characteristics of the TJ as employed in solar cells. The negative voltage represents the reverse bias operation of TJ as used in epitaxial stacking of optical cavities in LDs, which is the aim of this study. This requires TJs with low specific resistance to efficiently scale LD output power with epitaxial stacking. The voltage transition is caused by the behavior of the TJ transitioning from the tunneling state to the exponential diode state since the negative resistance region cannot be observed due to using a current source. Available voltage sources do not have the required current limit to provide such a high J_p; hence, a current source was employed.

The simulation results represented by the dotted lines are attained by using the nonlocal band-to-band and trap-assisted tunneling models assuming zero contact resistance [25], [26]. The intrinsic parameters, such as the effective mass of electrons (m_e) and holes (m_h), were modified as $m_e = 0.09$ and $m_h = 0.53$ to match the measured value of the peak current density for the n-doping concentration of 4.0×10^{19} cm^{-3}. The experimental J_p improved from 2.8×10^3 to 7.7×10^3 A/cm^2, with the n-doping concentration increasing from 4×10^{19} to 6×10^{19} cm^{-3}. The simulated n-doping concentrations of 5.0×10^{19} and 6.0×10^{19} cm^{-3} were adjusted to the value of 4.65×10^{19} and 4.80×10^{19}

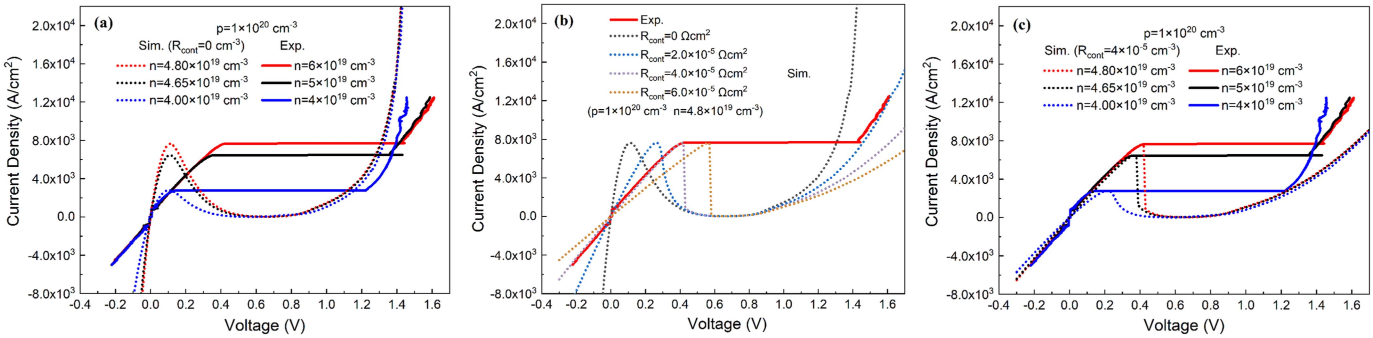

Fig. 2. Simulated J-V curves (dotted line) and experimental J-V curves (solid line) (a) for different n-doping concentrations with $R_{cont} = 0$ in the simulation, and (b) for $n = 6 \times 10^{19}$ cm^{-3} experiments result and $n = 4.8 \times 10^{19}$ cm^{-3} simulation results with different contact resistances, (c) for different n-doping concentrations with $R_{cont} = 4.0 \times 10^{-5}$ Ωcm^2 in the simulation.

cm^{-3}, respectively, to match J_p with the experimental results. Both simulation and experimental results demonstrate that J_p improves significantly with increasing doping concentration. However, the simulations show that lower doping concentrations are required to reach the experimental J_p values, which can be attributed to doping saturation. Excessive doping could also cause epitaxial degradation. Hence, we limited our study to the n-doping level of 6×10^{19} cm^{-3}.

The series resistance was previously studied [27] to show its effect on the J–V curve. Similarly, in Fig. 2(b), we examine the effect of the series resistance on the J–V curve by introducing an additional resistor into simulations to fit the experimental data [25], [28]. We separate the diode resistance into two series-connected resistances: TJ specific resistance R_{TJ} and a contact resistance R_{cont}. Then, by applying Ohm's law, the peak voltage V_p can be given as [25]

$$V_p = R_{TJ} J_P + R_{cont} J_P \tag{1}$$

where J_p is the peak current density with the corresponding voltage of V_p. Since J_p and R_{TJ} are independent of R_{cont} [27], we can obtain the contact resistance by varying its value to match V_p. Fig. 2(b) shows the simulation results with different R_{cont} values. As anticipated, J_p does not change with R_{cont}. The addition of this resistance leads to similar trends for the simulation and experimental results with a matching V_p for a contact resistance of $R_{cont} = 4.0 \times 10^{-5}$ Ωcm^2 at $V_p = 0.42$ V and $J_p = 7.7 \times 10^3$ A/cm^2. The experimentally measured total resistance of 5.5×10^{-5} Ωcm^2 is obtained by the slope of the J-V curve in the ohmic region, which is set by J_p and V_p. Then, the specific resistance of TJ can be extrapolated as 1.5×10^{-5} Ωcm^2, comparable to the best values for the TJs employed in ultra-high concentration multijunction solar cells [22]. As demonstrated in the simulation and experimental results of Fig. 2(a), the reverse-bias current density from −0.2 V to 0 V is similar to the forward-bias operation. Therefore, such a low TJ resistance is favorable for the laser diode with TJ operating in reverse bias. Since the TJ with a doping concentration of $n = 6 \times 10^{19}$ cm^{-3} and $p = 1 \times 10^{20}$ cm^{-3} provides desirable outcomes, they are used in the epitaxially stacked LDs.

To analyze the influence of the resistance for various n-doping levels, Fig. 2(c) presents the simulation results with the $R_{cont} =$

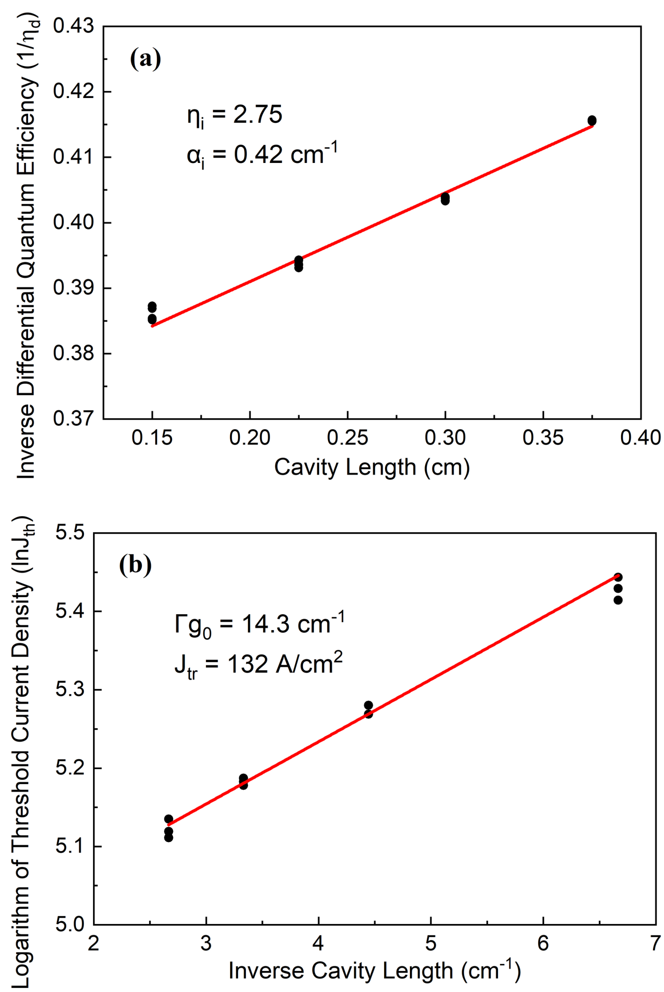

Fig. 3. Experiment results for (a) the inverse differential quantum efficiency versus cavity length, (b) the logarithm of threshold current density versus inverse cavity length.

4.0×10^{-5} Ωcm^2. It shows that the differences in the simulated total resistance values are much lower compared to zero contact resistance due to its dominating effect compared to TJ resistance. The simulation results agree with the experimental values to a large extent.

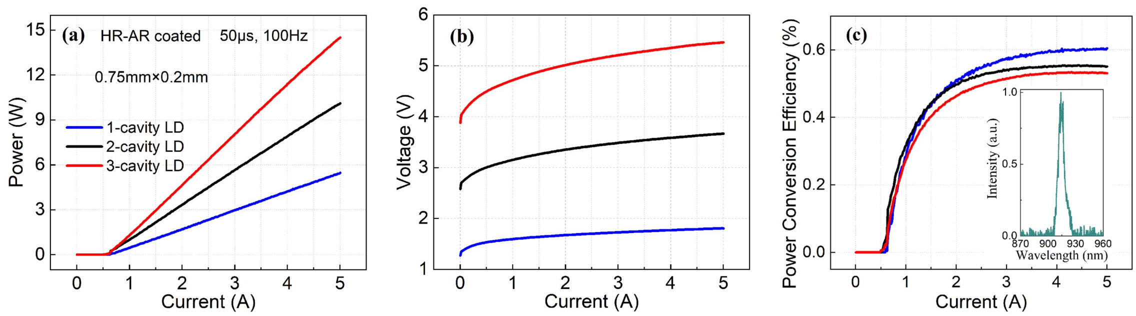

Fig. 4. (a) P-I, (b) V-I, (c) η-I curves with 1-, 2- and 3-cavity diode lasers. The inset in (c) shows a typical spectrum of 3-cavity laser at 5 A.

III. Laser Characterization Results

Uncoated 3-junction laser chips with 200 μm stripe width and four different cavity lengths were tested under QCW operation (50 μs, 100 Hz) to extract the internal parameters of the epitaxial structure. The dependencies of the inverse differential quantum efficiency ($1/\eta_{\mathrm{d}}$) on the cavity length (L) and the logarithm of the threshold current density ($\ln(J_{\mathrm{th}})$) on the inverse cavity length (1/L) are shown in Fig. 3(a) and 3(b). By linear fitting the data of 5 points for each length, the internal quantum efficiency η_{i}, internal optical loss α_{i}, transparency current density J_{tr}, and modal gain coefficient Γg_0 can be determined according to the equations [29]:

$$\frac{1}{\eta_d} = \frac{1}{\eta_i} + \left[\frac{1}{\eta_i}\frac{2\alpha_i}{\ln(1/R_1R_2)}\right]\cdot L \quad (2)$$

$$\ln J_{th} = \left[\ln J_{tr} + \frac{\alpha_i}{\Gamma g_0}\right] + \left[\frac{\ln(1/R_1R_2)}{2\Gamma g_0}\right]\cdot\frac{1}{L} \quad (3)$$

where the uncoated facet reflectivity R_1 and R_2 are assumed to be 0.32. The internal quantum efficiency η_{i} is 275% for the 3-cavity LDs, equivalent to 92% for each cavity on average. The low internal optical loss of 0.42 cm^{-1} confirms the high optical quality of the p-i-n epitaxial structure and its effective integration with the TJ structures. This also indicates that the optical loss contribution of the TJs is insignificant in agreement with the negligible overlap of the optical mode with the TJs. The relatively high transparency current density of 132 Acm^{-2} is due to employing double quantum wells, which are used to obtain the high modal gain coefficient Γg_0 of 14.3 cm^{-1} to compensate for the short cavity length.

Single emitter LDs with a cavity length of 0.75 mm and stripe width of 200 μm were cleaved, passivated, and coated with appropriate dielectric films. The reflectivity values are 95% for the high-reflective (HR) back-facet and 15% for the anti-reflective (AR) front-facet. As shown in Fig. 4, the power, voltage, and power conversion efficiency of 1-, 2-, and 3-cavity LDs were obtained under QCW conditions (50 μs, 100 Hz) up to 5 A before packaging. Fig. 4(a) shows the L-I (i.e., power-current) characteristics of 1-, 2- and 3-cavity LDs with an output power of 5.4, 10.1, and 14.5 W at 5 A, respectively. The corresponding slope efficiencies are 1.24, 2.29, and 3.36 W/A. The linear scaling of power and slope efficiencies indicates that the TJ is working properly. Fig. 4(b) shows the V-I curves, and the corresponding voltages at 5 A are 1.81, 3.64, and 5.46 V, demonstrating proper voltage scaling. The power conversion efficiency (PCE) in Fig. 4(c) shows a downward trend as the number of junctions increases. The PCE of 1-, 2- and 3-cavity laser diodes at 5 A are 60.3%, 55.0% and 53.1%, respectively. It is possibly caused by the weakening of the carrier and optical field confinement in the lateral direction as the number of cavities increases. This issue can be addressed by proper deep ion implantation of the structure to improve the carrier confinement; then, comparable efficiencies can be realized for different cavities. The inset in Fig. 4(c) illustrates a typical spectrum of the 3-cavity LD at 5 A.

To enable high current testing and operation of these devices, 3-cavity LDs are packaged as chip-on-board (COB). Fig. 5(a) shows the L-I characteristic of these lasers under short pulse test conditions of 100 ns and 100 Hz at 25 °C. The maximum output power of 83.1 W is attained at 30 A, which is limited by the driver current. The power measurement is not accessible at a low current for the same reason. The device has high a slope efficiency of 2.73 W/A, which is lower than the unpackaged chips. The possible reasons may be the lateral carrier leakage and higher optical loss at higher injection current. Another possibility is the pulse shape deformation due to inductive effects. Then, the actual pulse width may be less than 100 ns resulting in a lower duty cycle and measured peak power. The lateral current expansion is severe in this 3-cavity LD as the current diffusion path is longer than that of the 1- and 2-cavity, and the two TJs with a high conductivity intensify this effect. We can see the apparent electroluminescence emission from three epitaxial stacked p-i-n junctions from the inset of Fig. 5(a) at 2A.

The far-field profiles of the 3-cavity LD chip are shown in Fig. 5(b) at 5 A (50 μs, 100 Hz). The FWHM angles of the vertical (fast-axis) and horizontal (slow-axis) far-fields are about 29° and 18°, respectively. The vertical far-field agrees with the near-field optical mode profile simulation results presented in Fig. 2(c). Since each waveguide is diffraction-limited in the vertical direction, it results in a single-mode far-field profile for the 3-cavity laser diode. The built-in refractive index ridge step has little impact on the bottom two cavities, and noticeable lateral carrier expansion influences the material gain profile at contact edges. Hence, higher order modes reach the threshold, yielding larger lateral far fields. Therefore, the horizontal divergence angle of the 3-cavity is larger than the 1-cavity case. Further improvement to obtain a smaller lateral far field and higher slope efficiency can be realized by suppression of lateral current

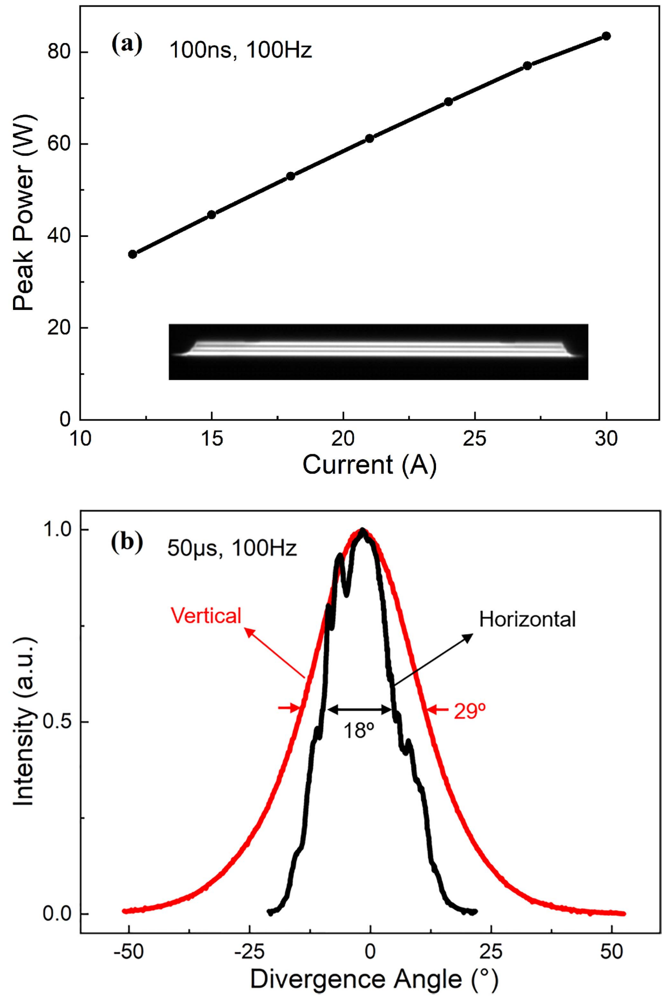

Fig. 5. For the 3-cavity laser diode COB: (a) L-I curve and lasing electroluminescence picture (inset). (b) Vertical and horizontal far-field.

spreading via lateral structuring techniques such as high-energy deep ion implantation [30], deep-etched index-guiding trenches, the enhanced self-aligned stripe technique [31], and lateral buried implantation structure [32].

IV. Conclusion

This work presented the GaAs TJ investigation and its integration into 3-cavity edge-emitting LDs. A high n-doping concentration of 6×10^{19} cm^{-3} and p-doping of 1×10^{20} cm^{-3} was used to realize a high peak current density of 7.7×10^4 A/cm^2 and a low specific resistance of 1.5×10^{-5} Ωcm^2, which are the best values achieved with GaAs-only TJs. Fabricated 1-, 2-, and 3-cavity LDs demonstrated power scaling with a high differential quantum efficiency of 275% and a low loss of 0.42 cm^{-1}, which is the lowest internal loss shown for a multiple cavity LD. The 3-cavity single emitter LD ($L = 750$ μm, $W = 200$ μm) was shown to reach a peak power of 83.1 W at 30 A (100 ns, 100 Hz), which is limited by the driver current. The dimensions are determined to obtain the smallest probable chip size for ∼100 W operation. It is possible to scale the power by increasing the LD size (i.e., longer cavity and/or broader waveguide) or by epitaxial stacking of more cavities in case of higher power requirements.

References

[1] P. W. Epperlein, *Semiconductor Laser Engineering, Reliability and Diagnostics: A Practical Approach to High Power and Single Mode Devices*, Hoboken, NJ, USA: Wiley, 2013.

[2] E. Zucker et al., "Advancements in laser diode chip and packaging technologies for application in kW-class fiber laser pumping," *Proc. SPIE*, vol. 8965, pp. 1–14, 2014, Art. no. 896507.

[3] V. Rossin et al., "High power, high brightness diode lasers for kW lasers systems," in *Proc. IEEE High Power Diode Lasers Syst. Conf.*, 2015, pp. 35–36.

[4] A. Klehr et al., "Wavelength stabilized high pulse power 48 emitter laser bars for automotive light detection and ranging application," *Semicond. Sci. Technol.*, vol. 35, no. 6, 2020, Art. no. 065016.

[5] A. Knigge et al., "Wavelength stabilized high pulse power laser bars for line-flash automotive LIDAR," *Proc. SPIE*, vol. 11262, pp. 1–12, 2020, Art. no. 112620F.

[6] A. Knigge et al., "Wavelength-stabilized high-pulse-power laser diodes for automotive LiDAR," *Physica Status Solidi*, vol. 215, no. 8, pp. 17004391–17004396, 2018.

[7] T. Hoffmann, A. Klehr, and A. Liero, "Compact high-current diode laser nanosecond-pulse source with high efficiency and 13 μJ output energy," *Electron. Lett.*, vol. 51, no. 1, pp. 83–85, 2015.

[8] C. P. Hsu et al., "A review and perspective on optical phased array for automotive LiDAR," *IEEE J. Sel. Topics Quantum Electron.*, vol. 27, no. 1, Jan./Feb. 2021, Art. no. 8300416.

[9] L. Esaki, "New phenomenon in narrow Germanium p−njunctions," *Phys. Rev.*, vol. 109, no. 2, pp. 603–604, 1958.

[10] A. Lyakh and P. Zory, "Gallium–Arsenide-based bipolar cascade lasers with deep quantum-well tunnel junctions," *IEEE Photon. Technol. Lett.*, vol. 18, no. 24, pp. 2656–2658, Dec. 2006.

[11] E. I. Davydova et al., "High-power laser diodes based on triple integrated InGaAs/AlGaAs/GaAs structures emitting at 0.9 μm," *Quantum Electron.*, vol. 39, no. 8, pp. 723–726, 2009.

[12] D. A. Vinokurov et al., "A study of epitaxially stacked tunnel-junction semiconductor lasers grown by MOCVD," *Semiconductors*, vol. 44, no. 2, pp. 238–242, 2010.

[13] M. Kanskar et al., "High power and high efficiency 1.8-kW pulsed diode laser bar," *J. Photon. for Energy*, vol. 7, no. 1, pp. 0160031–0160038, 2017.

[14] Y. Zhao et al., "High efficiency 1.9 kW single diode laser bar epitaxially stacked with a tunnel junction," *IEEE Photon. J.*, vol. 13, no. 3, Jun. 2021, Art. no. 1500708.

[15] S. O. Slipchenko et al., "Tunnel-coupled laser diode microarray as a kW-level 100-ns pulsed optical power source (λ = 910 nm)," *IEEE Photon. Technol. Lett.*, vol. 34, no. 1, pp. 35–38, Jan. 2022.

[16] N. Kageyama et al., "Development of high-power quasi-CW laser bar stacks with enhanced assembly structure," *IEEE Photon. Technol. Lett.*, vol. 28, no. 9, pp. 983–985, May 2016.

[17] Product features, Nanostack Pulsed Laser Diode in TO-56 pacakge 905 nm, Oct. 9 2022. [Online]. Available: https://ams-osram.com/products/lasers/ir-lasers-eel/osram-metal-can-to56-spl-tl90at08

[18] H. Wenzel, A. Maaßdorf, C. Zink, D. Martin, M. Weyers, and A. Knigge, "Novel 900 nm diode lasers with epitaxially stacked multiple active regions and tunnel junctions," *Electron. Lett.*, vol. 57, no. 11, pp. 445–447, 2021.

[19] H. Wenzel et al., "Internally wavelength stabilized 910 nm diode lasers with epitaxially stacked multiple active regions and tunnel junctions," *Electron. Lett.*, vol. 58, no. 3, pp. 121–123, 2021.

[20] T. Knödl, M. Golling, A. Straub, R. Jager, R. Michalzik, and K. J. Ebeling, "Multistage bipolar cascade vertical-cavity surface-emitting lasers: Theory and experiment," *IEEE J. Sel. Topics Quantum Electron.*, vol. 9, no. 5, pp. 1406–1414, Sep./Oct. 2003.

[21] Y. Onishi et al., "Long-wavelength gainnas vertical-cavity surface-emitting laser with buried tunnel junction," *IEEE J. Sel. Topics Quantum Electron.*, vol. 15, no. 3, pp. 838–843, May–Jun. 2009.

[22] I. García, I. Rey-Stolle, and C. Algora, "Performance analysis of AlGaAs/GaAs tunnel junctions for ultra-high concentration photovoltaics," *J. Phys. D: Appl. Phys.*, vol. 45, no. 045101, pp. 1–8, 2012.

[23] Y. Liu et al., "48 W continuous-wave output from a high-efficiency single emitter laser diode at 915 nm," *IEEE Photon. Technol.*, vol. 34, no. 22, pp. 1218–1221, Nov. 2022, doi: 10.1109/LPT.2022.3207786.

[24] J. Wheeldon et al., “Performance comparison of AlGaAs/GaAs and InGaP tunnel junctions for concentrated multijunction solar cells,” *Prog. Photovolt.: Res. Appl.*, vol. 19, pp. 442–452, 2011.

[25] M. Baudrit and C. Algora, “Tunnel diode modeling, including nonlocal trap-assisted tunneling: A focus on III–V multijunction solar cell simulation,” *IEEE Trans. Electron Devices*, vol. 57, no. 10, pp. 2564–2571, Oct. 2010.

[26] A. W. Walker, O. Thériault, M. M. Wilkins, J. F. Wheeldon, and K. Hinzer, “Tunnel-junction-limited multijunction solar cell performance over concentration,” *IEEE J. Sel. Topics Quantum Electron.*, vol. 19, no. 5, Sep./Oct. 2013, Art. no. 4000508.

[27] W. Guter and A. W. Bett, “I-V characterization of tunnel diodes and multijunction solar cells,” *IEEE Trans. Electron Devices*, vol. 53, no. 9, pp. 2216–2222, Sep. 2006.

[28] M. Hermle, G. Leray, S. P. Philipps, and A. W. Bett, “Numerical simulation of tunnel diodes for multi-junction solar cells,” *Prog. Photovolt.: Res. Appl.*, vol. 16, pp. 409–418, 2008.

[29] Y. Liu et al., “High-power operation and lateral divergence angle reduction of broad-area laser diodes at 976 nm,” *Opt. Laser Technol.*, vol. 141, no. 15, 2021, Art. no. 1071451.

[30] M. Winterfeldt et al., “High beam quality in broad area lasers via suppression of lateral carrier accumulation,” *IEEE Photon. Technol. Lett.*, vol. 27, no. 17, pp. 1809–1912, Sep. 2015.

[31] M. Elattar et al., “High-brightness broad-area diode lasers with enhanced self-aligned lateral structure,” *Semicond. Sci. Technol.*, vol. 35, 2020, Art. no. 095011.

[32] P. Della Casa et al., “High power broad-area lasers with buried implantation for current confinement,” *Semicond. Sci. Technol.*, vol. 34, no. 10, 2019, Art. no. 105005.